ACS APPLIED MATERIALS & INTERFACES

Research Article

www.acsami.org

Graphene Aerogels Decorated with α-FeOOH Nanoparticles for Efficient Adsorption of Arsenic from Contaminated Waters

Ivan Andjelkovic,*[,†,‡] Diana N. H. Tran,[‡] Shervin Kabiri,[‡] Sara Azari,[‡] Marijana Markovic,[§] and Dusan Losic*[,‡]

[†]Innovation Center of the Faculty of Chemistry, University of Belgrade, Studentski Trg 12-16, Belgrade, Serbia

[‡]School of Chemical Engineering, The University of Adelaide, Adelaide, SA 5005, Australia

[§]Institute of Chemistry, Technology and Metallurgy, Center of Chemistry, University of Belgrade, Njegoseva 12, Belgrade, Serbia

Supporting Information

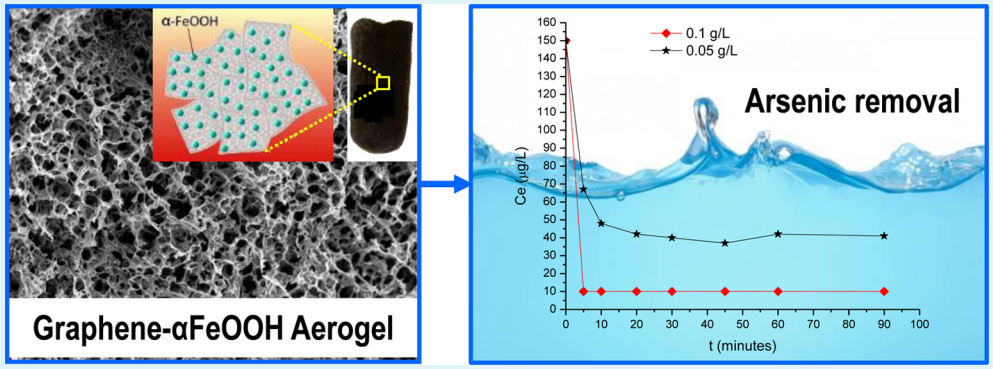

ABSTRACT: Arsenic (As) is the world's most hazardous chemical found in drinking water of many countries; therefore, there is an urgent need for the development of low-cost adsorbents for its removal. Here, we report a highly versatile and synthetic route for the preparation of a three-dimensional (3D) graphene−iron oxide nanoparticle aerogel composite for the efficient removal of As from contaminated water. This unique three-dimensional (3D) interconnected network was prepared from natural graphite rocks with a simple reaction, without the use of harsh chemicals, which combines with the exfoliation of graphene oxide (GO) sheets via the reduction of ferrous ion to form a graphene aerogel composite decorated with iron oxide nanoparticles. The prepared adsorbent showed outstanding absorption performance for the removal of As from contaminated water, because of its high surface-to-volume ratio and characteristic pore network in the 3D architecture. The performed case study using real drinking water contaminated with As under batch conditions showed successful removal of arsenic to the concentration recommended by the World Health Organisation (WHO).

KEYWORDS: *graphene, α-FeOOH nanoparticles, aerogel, adsorption, arsenic*

INTRODUCTION

Arsenic (As) is known as one of the most toxic chemical elements at very low concentrations; for centuries, it has been considered to be synonymous with toxicity. Arsenic contamination of drinking and environmental waters has led to a massive epidemic of arsenic poisoning and presents a considerable health problem around the world, affecting more than 100 million people drinking contaminated waters.[1] The predominant form of inorganic arsenic in oxic, aqueous environments is arsenate [As(V) as H_3AsO_4, $H_2AsO_4^-$, $HAsO_4^{2-}$, and AsO_4^{3-}], whereas arsenite [As(III) as $H_3AsO_3$and $H_2AsO_3^-$] is more prevalent in anoxic environments.[2] Their higher concentration in environmental waters can be a result of natural or industrial contaminations. The consumption of arsenic in drinking water is a serious dilemma, which could cause death and severe health problems, such as anemia and leukemia,[3] peripheral neuropathy,[4] hypertension,[5] cardiac vascular diseases,[6] respiratory diseases,[7] diabetes mellitus,[8] and malignancies, including cancer of the lungs and bladder,[9] liver,[10] and skin.[11]

Many technologies were explored for arsenic removal from contaminated waters, including adsorption using different types of adsorbents; precipitation with alum, iron, and iron/manganese (Fe/Mn); lime softening; reverse osmosis; electrodialysis; ion exchanges; membrane filtration; and biological remediation.[12] Among them, the adsorption methods emerged as the most promising technology, because of the low cost, simplicity of the procedure and possibility to be applied to individual household systems.[13−15] The benchmark for all of these technologies is lowering the recommended maximum

Received: February 20, 2015
Accepted: April 14, 2015
Published: April 14, 2015

DOI: 10.1021/acsami.5b01624
ACS Appl. Mater. Interfaces 2015, 7, 9758−9766

concentrations of arsenic in drinking water below 10 ppb (as stated by WHO), which is considered to cause health problems.[16] Numerous different types of adsorbents were explored and developed in the past years, but with different efficiencies to remove arsenic, which requires more research to address this problem. Among the most examined materials for arsenic removal are metal oxides/hydroxides,[17−21] activated carbon,[22,23] zeolites,[24] and industrial waste.[25−27] Faria et al.[20] used ultrafine δ-FeOOH particles for As(V) adsorption, where it was found that, at neutral pH, the adsorption capacity of 37.3 mg/g was assigned to the small particle size and the high specific surface area of δ-FeOOH. Experiments with activated carbon showed that after pretreatment of activate carbon with Cu(II) solution[22] or after impregnation with metallic silver or copper[23] better removal of arsenic was achieved. Fly ash, collected from a sub-bituminous coal-combustion plant in Southland, New Zealand, provided removal efficiency of As(V) in the range of 83%−91%. Possible species responsible for arsenic adsorption could be calcium minerals and amorphous iron and aluminum hydroxides, which are present in fly ash in high content.[25] The requirement for all these adsorbent are high and fast removal of arsenic in the water without expensive pretreatment, low cost and availability of raw materials, simple, scalable and sustainable procedure for their production and low price of the adsorbent.

Graphene, because of its enormous specific surface area (2600 m^2/g), good mechanical stability, the flexibility to tailor its surface chemistry, and the possibility of a large-scale production from natural sources (graphite), has received considerable research attention to develop advanced adsorbents for environmental applications.[28−30] Graphene and graphene-based materials (GBM) have proved to be good candidates to act as a support for nanoparticles immobilization, which enables the combined and synergistic actions that is highly desired for advance adsorption performance. One of the first attempts to use graphene composite for arsenic removal is reported by Chandra et al.,[31] who synthesized water-dispersible magnetite-reduced graphene oxide composites (M-GRO) which are removed after the treatment of water with a magnet. Several other iron-decorated graphene oxide (GO) materials have also been reported for the effective removal of arsenate from contaminated drinking water.[32] Because it is usually easier to remove As(V) then As(III) from water, many authors have modified carbon-based materials with groups that have oxidizing power, such as manganese dioxide (MnO_2) or titanium dioxide (TiO_2), in order to oxidize and remove arsenic from water.[33−35] However, some of these methods involve the use of toxic substances and are not reliable for scalable production. Cong et al.[36] recently synthesized in a single step, without the use of hazardous materials, a self-assembled graphene-αFeOOH hydrogel, which demonstrated large sorption capacity toward chromium (Cr) and lead (Pb) ions in aqueous solution. In our previous work, we demonstrated a similar procedure and synthesized graphene/carbon nanotubes aerogel decorated with iron oxide nanoparticles and showed their exceptional performance for the removal of oil from water.[37]

In this work, we present a simple approach to engineer graphene-iron nanoparticle aerogels for the adsorption of arsenic in drinking water. The scheme of the synthetic process is summarized in Figure 1. GO that has been prepared from natural graphite rocks, and ferrous sulfate, were used as the starting materials. The reduction of GO to graphene and the formation of the graphene network hydrogel was performed by the Fe ions upon heating, therefore eliminating the use of toxic chemicals in the process, usually used for GO reduction.[38] The existence of abundant polar oxygen-containing groups on the GO sheets such as epoxy, carboxyl, and hydroxyl can induce diffusion of ferrous ions toward the GO sheets by electrostatic interaction, which is oxidized into ferric ions by the oxygen containing groups on the surface of GO. At the same time, the self-assembling of reduced GO sheets anchored with iron (Fe) nanoparticles (FeNPs) into the hydrogel with interconnected networks is driven by the combined hydrophobic and $\pi-\pi$ stacking interactions, because of the decrease of oxygenated groups on the GO surface. The deposited nanoparticles on the surface of the reduced GO sheets serve as spacers that effectively avoid aggregation of the graphene sheets during the reduction process. The formed three-dimensional (3D) hydrogel is finally transformed to an aerogel by freeze-drying to form a graphene-FeNP aerogel (Figure 1d). Numerous characterization methods, such as scanning electron microscopy (SEM), transmission electron microscopy (TEM), Fourier transform infrared spectroscopy (FTIR), and Raman spectroscopy were performed to confirm the 3D structure and chemical composition of the prepared aerogels. Their adsorption properties for arsenic were explored using inductively coupled plasma atomic emission spectroscopy (ICP-AES) by a series of experiments to test the batch adsorption using a model As solution, followed by testing with a real sample of drinking water contaminated with As.

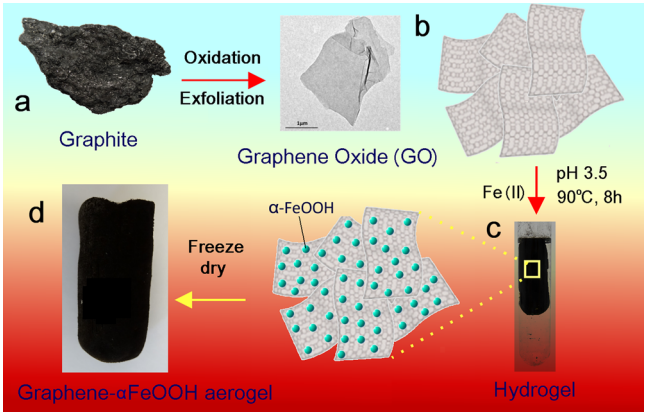

Figure 1. Schematic diagram of the synthesis process of the anchored α-FeOOH nanoparticles onto reduced GO sheets: (a) graphite ore, (b) GO sheets, (c) formation of hydrogel after reaction, and (d) graphene−α-FeOOH aerogel (GN-α-FeOOH aerogel) after freeze-drying.

EXPERIMENTAL SECTION

Materials and Chemicals. Natural graphite rocks (Uley, Eyre Peninsula, South Australia) is supplied from a local mining site and milled into a fine powder using a benchtop ring mill (Rocklabs). Iron sulfate ($FeSO_4 \cdot 7H_2O$, Sigma−Aldrich), potassium permanganate ($KMnO_4$, Sigma−Aldrich), sulfuric acid (98%, H_2SO_4, Chem-Supply), phosphoric acid (85% w/w, H_3PO_4, Chem-Supply), hydrogen peroxide (30%, H_2O_2, Chem-Supply), hydrochloric acid (35%, HCl, Chem-Supply), ammonium solution (30%, NH_4OH, Chem-Supply), sodium hydroxide (NaOH, Chem-Supply), and ethanol (Chem-Supply) were used directly without further purification. Arsenite and arsenate stock solutions (1 g/L) were prepared

DOI: 10.1021/acsami.5b01624
ACS Appl. Mater. Interfaces 2015, 7, 9758−9766

by dissolving an appropriate amount of $NaAsO_2$ (Fisher Scientific, USA) and $Na_2HAsO_4{\cdot}7H_2O$ (Fluka, Spain) in deionized water (DI), respectively. High-purity Milli-Q water (18.2 MΩ cm at 25 °C, pH 5.6) was used throughout the study, unless otherwise stated.

Preparation of Graphene Oxide (GO). Graphene oxide was prepared via the oxidation of natural graphite, according to the improved Hummer's method.[39] Briefly, a 9:1 mixture of concentrated sulfuric acid and phosphoric acid (240:27 mL) was cooled to 4 °C. Under stirring at room temperature, the cooled acid mixture was added slowly to the graphite powder (2 g) and potassium permanganate (12 g) then heated to 50 °C for about 12 h, forming a thick paste. The reaction was cooled to room temperature and poured onto ice (300 mL) with hydrogen peroxide (2 mL). The mixture was then first washed with distilled water, second with hydrochloric acid (32%) and finally twice with ethanol. For each successive wash the product was centrifuged at 4200 rpm for 2 h where the product was removed from the supernatant. The obtained light brown GO then was vacuum-dried overnight at 45 °C.

Preparation of GN-α-FeOOH Aerogels. In a typical procedure, 20 mg of GO was sonicated for 30 min in 10 mL of water until a uniform and homogeneous solution was obtained.[36] Following the addition of 1 mmol ferrous sulfate, the solution was further sonicated for 30 min and the pH was adjusted to 3−3.5 with HCl. The solution was transferred to a cylindrical glass vial, which was placed into a 90 °C oil bath for 8 h without stirring to form the graphene hydrogel. The resulted hydrogel was washed with DI water a few times to remove any outside impurities and freeze-dried under −30 °C and at 600 μbar pressure to obtain the corresponding graphene aerogel. The schematic procedure for the graphene-iron hybrid aerogel is represented in Figure 1.

Characterizations. All the prepared materials including GO, and the GN-α-FeOOH aerogel were characterized by several characterization techniques. The morphology of the samples was characterized via SEM analysis (Model Quanta 450, FEI, USA) and TEM analysis (FEI Tecnai G2 Sprit). FTIR analysis (Spectrum 100, Perkin−Elmer) was used to identify the functional groups of the resulted materials scanned in the range of 500−4000 cm^{-1} in transmission mode. The vibrational characteristic of the samples were analyzed via Raman spectroscopy (LabRAM HR Evolution, Horiba Jvon Yvon, Japan) using a 532 nm laser as the excitation source in the range of 800−3000 cm^{-1}. A 100× objective was used with a 300 μm confocal spot size. Each spectrum was measured using an integration time of 10 s for 3 accumulations. The X-ray diffraction (XRD) (Model Miniflex 600, Rigaku, Japan) measurement was performed from 2θ = 5°−80° to illuminate the composition of the 3D graphene aerogel at a scan rate of 5°/min. The zeta potential of the prepared aerogel was also measured in triplicate with a Malvern Zetasizer (Nanoseries, Australia) as a function of pH. The aerogels were uniformly crushed up then dispersed in water with 10 mmol NaCl (Chem-Supply). The pH of the mixture was adjusted with either HCl or NH_4OH from 3 to 10.

The specific surface area (SSA) of the prepared GN-α-FeOOH aerogel was determined using the Methylene Blue (MB) adsorption method by ultraviolet−visible (UV-vis) spectroscopy (Model UV-1601, Shimadzu, Japan). The MB method is widely accepted in the literature as a more reliable method for determining the surface area of graphene-based 3D materials, compared with the BET nitrogen adsorption method.[40,41] Details are provided in the Supporting Information.

Adsorption of As ions by GN-α-FeOOH Aerogels. Batch adsorption tests were carried out individually for As(III) and As(V) to examine the effect of contact time and pH on As adsorption, and to determine the adsorption capacity of the adsorbent. Experiments were performed in 250 mL conical flasks with 5 mg of adsorbent and 100 mL of arsenic solution in DI water at room temperature (20 °C ± 2) that were placed on a shaker (IKA KS260 basic, Germany) and mixed at 300 rpm.

For kinetic experiments, 5 mg/L arsenic solutions with initial pH 7 were mixed for 5, 10, 15, 20, 30, 45, 60, and 120 min. After the specified contact time, the suspensions were immediately filtered through a 0.45 μm filter paper and the arsenic concentrations were measured with inductively coupled plasma−atomic emissions spectroscopy (ICP-AES) (Model iCap 6500Duo, Thermo Fisher, U.K.).

The effect of pH on arsenic adsorption was examined in pH range of 3−11. The initial pH of the arsenic solution (5 mg/L) was adjusted using diluted HCl or NaOH solution. After the addition of the adsorbent and the solutions were mixed for 60 min, the suspensions were immediately filtered through a 0.45 μm filter paper and the filtrates were analyzed.

Isotherm studies were carried out at initial pH 9 and 8 for As(III) and As(V), respectively. Experiments were performed by mixing different concentrations of As(III) and As(V) with a constant dose of adsorbent (0.05 g/L) for 60 min. The arsenic concentrations were in the range of 1−16 mg/L.

Finally, the case study experiments were performed using a sample of drinking tap water from the city of Zrenjanin (Serbia), which is known to have a high concentration of arsenic. After the sampling water was immediately stored at 4 °C, the experiments were carried out within 48 h. Kinetic experiments were performed with 100 mL of the natural water with two dosages of adsorbent (0.05 and 0.1 g/L). After the specified mixing time, the suspensions were filtered through a 0.45 μm filter and the concentration of arsenic was measured. All experiments were performed in triplicates and the average values were presented with a maximum deviation of 8%, if error bars are not shown.

RESULTS AND DISCUSSION

Structural and Chemical Characterization of GN-α-FeOOH Aerogels. A black, light and porous GN-αFeOOH aerogel obtained after the freeze-drying process is shown in Figure 2a. The internal structure of the prepared aerogel is presented by a series of SEM and TEM images in Figures 2a−e. The low-magnification SEM image (Figure 2a) shows the well-defined and interconnected 3D network of the graphene nanosheets with macrometer pore sizes. EDAX results clearly show that the graphene aerogels contain iron oxide nanoparticles (Figure 2c). A large number of nanoparticles dispersed on the graphene sheets were observed in the magnified SEM image (Figure 2b) and TEM images (Figures 2d and 2e). The TEM images show that the α-FeOOH nanoparticles are indeed randomly dispersed onto the thin graphene sheets, as nanoparticles with irregular shapes and dimensions from 10 nm to 50 nm.

To further confirm the formation of the FeOOH nanoparticles on the reduced GO sheets, XRD analysis was conducted. Figure 3a shows the XRD plots of the GN-α-FeOOH aerogel compared to GO, which was used as a reference. GO has a characteristic strong peak at 2θ = 11.2°

DOI: 10.1021/acsami.5b01624
ACS Appl. Mater. Interfaces 2015, 7, 9758−9766

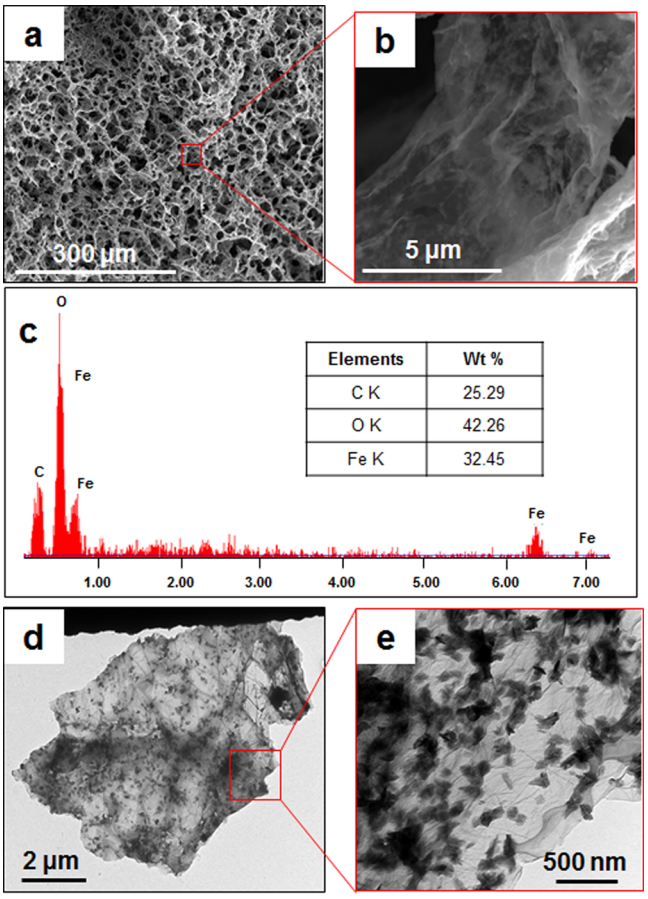

Figure 2. SEM images of the prepared GN-αFeOOH aerogel showing (a) low magnification and (b) high magnification of the typical network structure, (c) EDAX of the prepared aerogel, and (d, e) low- and high-magnification TEM images of the graphene sheets showing the presence of α-FeOOH nanoparticles and their typical structure, respectively.

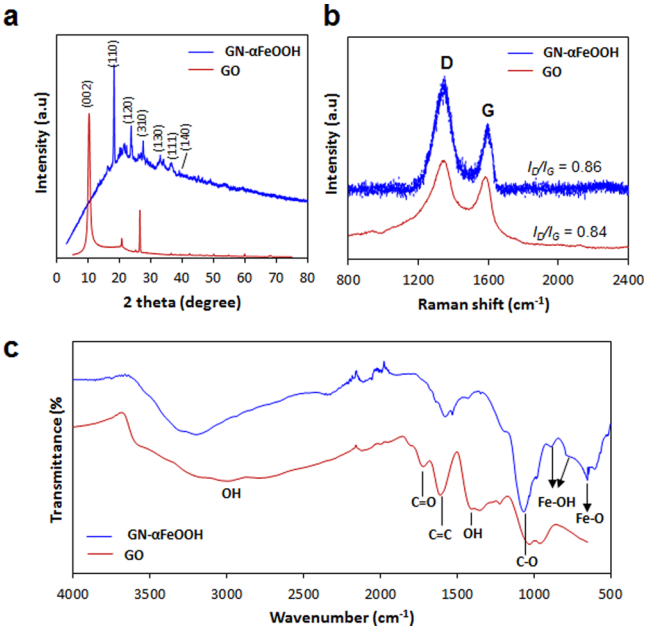

Figure 3. (a) XRD, (b) Raman, and (c) FTIR spectra of the GO and GN-α-FEOOH aerogel.

(002), indicating the presence of an interlayer *d*-spacing (0.79 nm). This spacing is attributed to the intercalation of water molecules and the formation of oxygen-containing functional groups on the GO sheets. GO also has a peak at $2\theta = 22.5°$, which indicates an incomplete oxidation of GO.[42] The strong peak of GO disappears after being reacted with $FeSO_4$; therefore, GO is reduced by $FeSO_4$. All peaks up to $2\theta = 20°$ in the XRD spectra of the GN-α-FeOOH aerogel are typical of the α-FeOOH diffraction peaks for goethite (Joint Committee on Powder Diffraction Standards File Card No. 9003076). No obvious diffraction peaks of graphene oxide were observed.

Raman spectroscopy is the most respectable tool that provides structural and quality characterization of the carbon surface. Two characteristic peaks are observed in the Raman spectra of GO, as shown in Figure 3b. The D-band (~1349 cm^{-1}) is characteristic of the defects and disorders caused by the graphene edges, and the G-band (~1597 cm^{-1}) is related to the vibration of sp^2 bonded carbon atoms in the carbon structure.[43] The Raman spectra of the GN-α-FeOOH aerogel shows a higher relative intensity and a higher disorder in the D-band (1357 cm^{-1}), because of the defects and vacancies left behind in the reduced graphene sheets. The intensity ratio of the D- and G-band (I_D/I_G) is a useful indicator to evaluate the ordered or disordered crystal structures of carbon. There is a slight increase in the I_D/I_G for the GN-α-FeOOH aerogel (0.86), compared to that of GO (0.84), confirming the increasingly disordered graphene sheets. The peak shifts in the D- and G-bands of the aerogel also reveals the charge transfer between the graphene sheets and α-FeOOH nanoparticles.[36]

The FTIR results of the GN-α-FeOOH aerogel (Figure 3c) showed good agreement with those obtained by XRD. The bands between 900 cm^{-1} and 500 cm^{-1} can be assigned to the Fe−OH bending vibrations and Fe−O stretching vibration, therefore indicating the presence of the α-FeOOH phase.[44] There is an obvious decrease in the oxygen functional groups of the carbonyl and epoxy in the FTIR plot of GO, indicating the effective reduction of the GO sheets. Based on the above results, it can be concluded that the co-assembly of graphene sheets and α-FeOOH nanoparticles is through the reduction of GO to graphene by Fe(II) and the hydrolysis of Fe(III) ions. The deposited α-FeOOH nanoparticles effectively served as spacers to stop the aggregation of the graphene sheets during the reduction process. In addition, the self-assembled GO sheets and α-FeOOH nanoparticles in the 3D interconnected hydrogel is also driven by the combined hydrophobic and π−π stacking interactions, because of the reduction of the oxygen-containing functional groups on the graphene surface.

Adsorption Capacity of Arsenic from Water. *Batch- and Diffusion-Based Adsorption.* The adsorption kinetics is one of the most important factors to describe the adsorbent's performance and the mechanism of adsorption that can be used for optimization and improvement of the removal process. Figure 4 shows adsorption graphs of As(III) and As(V) removal by the prepared GN-α-FeOOH aerogel. These graphs confirm that the initial adsorption for both type of arsenic species is very fast. Most of the As(III) was adsorbed within the first 5 min, while for As(V) the adsorption increased almost linearly with time until 60 min from where equilibrium was achieved, for both As(III) and As(V). The fast kinetics of both types of arsenic species can be explained by the well-developed mesopores, micropores, and high surface area of the GN-α-FeOOH adsorbent. The specific surface area of the prepared adsorbent was calculated to be 220 ± 5 m^2/g. The greater

DOI: 10.1021/acsami.5b01624
ACS Appl. Mater. Interfaces 2015, 7, 9758−9766

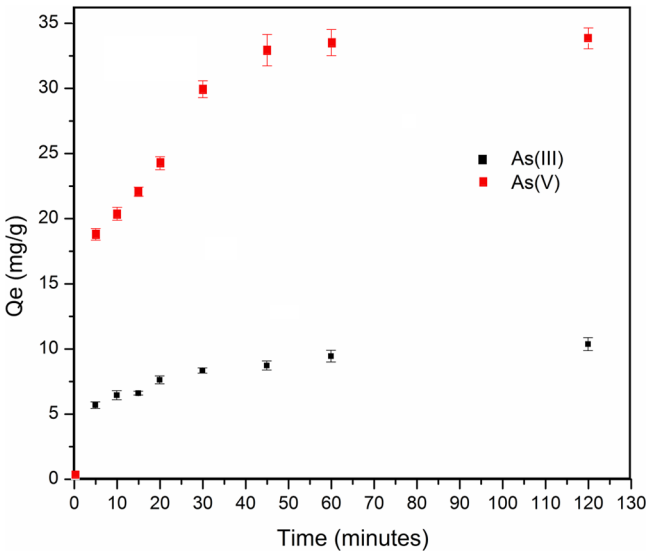

Figure 4. Kinetics of As(III) and As(V) removal by the GN-α-FeOOH aerogel. Conditions: arsenic concentration for both type of arsenic species = 5 mg/mL, pH 7.

porous structure of the prepared aerogel is due to the Fe particles acting as spacers in the graphene sheets. Also, a higher uptake in As(V) (33.8 mg/g) than As(III) (10.3 mg/g) was noticed.

Two kinetic models were further applied for determining the rate of As(III) and As(V) adsorption, pseudo-first-order and pseudo-second-order kinetic models. Pseudo-first-order rate expression of the Lagergren equation[45] is given as

$$\log(Q_e - Q_t) = \log Q_e - k_1 t$$

where Q_e and Q_t are the amount of arsenic adsorbed (in mg/g) at equilibrium and at time t (min), respectively, and k_1 (min^{-1}) is the rate constant of the pseudo-first-order adsorption. The adsorption rate constant can be determined from the slope of the linear plot of $\log(Q_e - Q_t)$ vs t.

Pseudo-second-order rate expression[46] is given as

$$\frac{t}{Q_t} = \frac{1}{Q_e^2 k_2} + \frac{t}{Q_e}$$

where k_2 (g mg^{-1} min^{-1}) is the pseudo-second-order rate constant and k_2 can be calculated from the slope and intercept of the plot of t/Q_t vs t.

The kinetics data obtained from the linearized plots for pseudo-first-order and pseudo-second-order kinetic models are presented in Table 1. The table shows that the pseudo-first-order model gives reasonably good R^2 values for As(III) and As(V) adsorption but higher R^2 values were achieved with the pseudo-second-order rate model for both types of arsenic species. In most cases, the pseudo-first-order model is suitable for the first 20−30 min of the adsorption process;[47] one of the drawbacks of this model is accurately determining Q_e, which is a rather difficult task. In our case, probably after the very fast initial response, the adsorption becomes very slow and an approximation must be made about Q_e introducing an element of uncertainty in the calculations. Under our experimental conditions, the pseudo-second-order model, which is interpreted as an example of chemical adsorption involving valence forces through sharing or exchange of electrons between adsorbent and metal ions, is a better approximation of the average reaction kinetic for both types of arsenic species.

Influence of pH. The influence of pH on arsenic adsorption is very important, because pH affects the speciation of arsenic species, as well as the surface properties of the GN-α-FeOOH adsorbent. Figure 5a presents the influence of pH on the adsorption of As(III) and As(V) species studied from pH 3 to pH 11. To better understand the interaction of different As species available at different pH, the E_h−pH diagram is presented in Figure 5b. Arsenic exists in the −3, 0, +3 and +5 oxidation states controlled by pH and redox potential with environmental forms including arsenious acids (H_3AsO_3, $H_2AsO_3^-$, $HAsO_3^{2-}$), arsenic acids (H_3AsO_4, $H_2AsO_4^-$, $HAsO_4^{2-}$), arsenites, arsenates, arsine, etc. A slow, linear increase of As(III) adsorption with an increase of pH from pH 3 to pH 9 with a slight decrease from pH 9 to pH 11 is observed. The possible reason for the increase of adsorption in this pH range could be due to the electrostatic attraction between the increasing number of anionic As(III) species, $H_2AsO_3^-$, and positively charged surface of the adsorbent. Above pH 9.2, As(III) exists mainly as $H_2AsO_3^-$ and the electrostatic repulsion with the negatively charged surface of the GN-αFeOOH aerogel could be responsible for the decrease of adsorption.[48]

In the case of As(V), the adsorption sharply increases with pH from pH 3 to pH 4, which is probably due to the increase of negatively charged As(V) species (Figure 5b). From pH 4 to pH 6, the adsorption of As(V) did not drastically change as the number of $H_2AsO_4^-$ also did not change. After pH 6, a slow rise in the As(V) adsorption with a maximum at pH 8 is observed. A noticeable decrease of adsorption was seen at pH 10 and a total inhibition of adsorption was encountered at pH 11. Similar results were also obtained by other researchers.[50,51] Arcibar-Orozco et al.[52] proposed two mechanisms that are responsible for the adsorption of arsenic onto iron-modified carbons: electrostatic attraction with surface groups and ligand interchange between arsenic and iron oxyhydroxide nanoparticles. From the determined isoelectric point (IEP), as the surface of the GN-α-FeOOH aerogel is negatively charged above pH 6.2 ± 0.1 (Figure 6) and the dominant species of As(V) are $H_2AsO_4^-$, $HAsO_4^{2-}$, and AsO_4^{3-} at pH 2.24, 6.76, and 11.60, respectively, we can conclude that, besides the electrostatic attraction, after pH 6, the ligand interchange is involved and is probably the dominant mechanism of arsenic adsorption to the GN-α-FeOOH aerogel.

Adsorption Isotherms. Freundlich[53] and Langmuir[54] models are the most used models for describing the adsorbed amount

Table 1. Kinetics Parameters for Adsorption of As(III) and As(V) on the GN-α-FeOOH Aerogel

	Pseudo-first order			Pseudo-second order		
element	k_1 (min^{-1})	Q_e (mg/g)	R^2	k_2 (g/mg min)	Q_e (mg/g)	R^2
As(III)	0.018 ± 0.001	4.86 ± 0.05	0.9656	0.011 ± 0.001	10.87 ± 0.13	0.9962
As(V)	0.036 ± 0.002	32.77 ± 0.30	0.9172	0.004 ± 0.000	36.10 ± 0.33	0.9961

DOI: 10.1021/acsami.5b01624
ACS Appl. Mater. Interfaces 2015, 7, 9758−9766

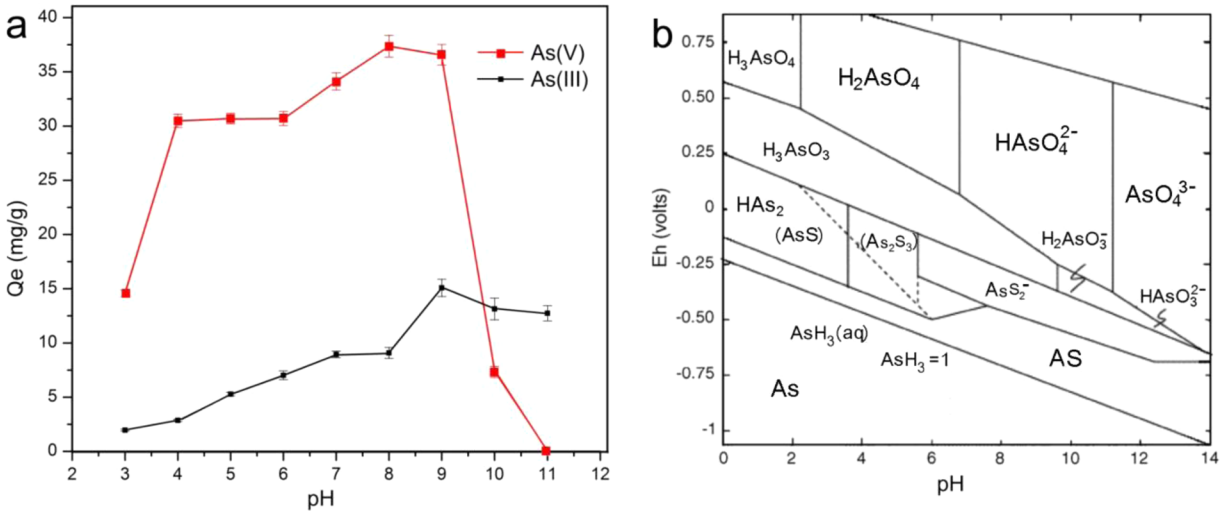

Figure 5. (a) The influence of pH on the adsorption of As(III) and As(V) by the graphene-α-FeOOH aerogel. Condition: Arsenic concentration for both types of arsenic species = 5 mg/L. (b) Arsenic speciation diagram with respect to E_h−pH values.[49]

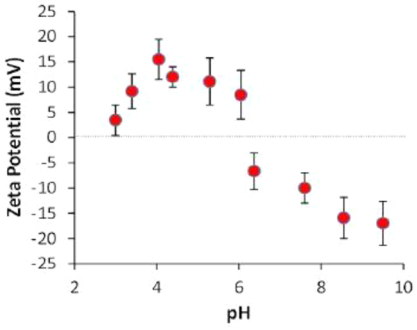

Figure 6. Zeta potential measurements of GN-α-FeOOH aerogels, as a function of pH.

(Q) and concentration in solution (C) at constant temperature (T).

The Freundlich model is given as

$$Q_e = K_f C_e^{1/n}$$

where Q_e (mg/g) is the amount of adsorbed arsenic per unit of adsorbent, K_f is the Freundlich constant related to adsorption capacity, C_e (mg/L) is the equilibrium arsenic concentration, and n is the dimensionless Freundlich constant, which indicates the intensity of adsorption.

The Langmuir isotherm model can be expressed as

$$\frac{C_e}{Q_e} = \frac{1}{K_L Q_o} + \frac{C_e}{Q_o}$$

where Q_o (mg/g) is the amount adsorbed per unit weight of adsorbent required for monolayer capacity and K_L (L/mg) is the Langmuir constant.

The parameters of the Freundlich and Langmuir adsorption isotherms are presented in Table 2. For the adsorption of As(III), better regression coefficient was obtained with the Freundlich isotherm model, which assumes multilayer adsorption on the energetically heterogeneous surface (see Figures S1 and S2 in the Supporting Information). As for adsorption of As(V), the Langmuir isotherm model, which assumes monolayer sorption on the homogeneous surface, describes the adsorption more accurately than the Freundlich model (see Figures S3 and S4 in the Supporting Information). This is in agreement with the results obtained for the effect of pH on adsorption of As(III) and As(V). Approximately 40% of As(III) at pH 9 is present as $H_2AsO_3^-$ and 60% as electroneutral H_3AsO_3, where they will attach to different active sites on the adsorbent. At pH 8, As(V) is present as negatively charged $H_2AsO_4^-$/$HAsO_4^{2-}$ species; therefore, adsorption at this pH probably occurs via a ligand exchange reaction with the hydroxide groups of α-FeOOH. Compared with similar materials, the prepared GN-α-FeOOH aerogel exhibited higher adsorption capacity for the removal of As(III) and As(V), as shown in Table 3.

Table 2. Freundlich and Langmuir Isotherm Parameters for Adsorption of As(III) and As(V) on the GN-α-FeOOH Aerogel

	Freundlich model		Langmuir model	
element	K_f (mg/g)	R^2	Q_o (mg/g)	R^2
As(III)	13.4 ± 1.2	0.9995	2.8 ± 0.4	0.8038
As(V)	1.8 ± 0.2	0.9636	81.3 ± 4.8	0.9855

Case Study. For examination of arsenic removal by the graphene−α-FeOOH aerogel in real life application, adsorption experiments were conducted on a natural water sample (tap water) from the city of Zrenjanin, which is located in the

Table 3. Comparison of Different Adsorbents Used for the Removal of Arsenic from Water

			Adsorption capacity (mg/g)		
adsorbent	pH	concentration range (mg/L)	As(III)	As(V)	reference
Fe_3O_4−RGO−MnO_2	7	0.01−10.0	14.04	12.22	55
M-RGO	7	3−7	13.10	5.83	31
magnetite-doped activated carbon fiber	4	0−7		4.16	56
magnetite−graphene−LDH	6			73.14	57
GN-α-FeOOH aerogel	8−9	1−16	13.42	81.3	this study

DOI: 10.1021/acsami.5b01624
ACS Appl. Mater. Interfaces 2015, 7, 9758−9766

northern part of Serbia. The underground water in some parts of this city is known to have high concentration of naturally contaminated As, which presents a serious problem. Table S1 in the Supporting Information shows the chemical composition of the natural tap water sample used in the experiments showing the concentration of arsenic, which exceeds 15 times the value recommended by WHO. Adsorption experiments for the removal of As from the natural water using the GN-α-FeOOH aerogel with two dosage rates is presented in Figure 7.

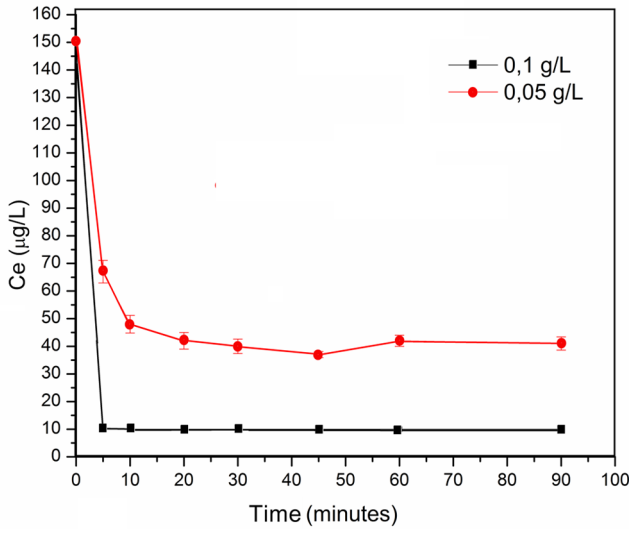

Figure 7. Removal of arsenic from the contaminated drinking water (city of Zrenjanin, Serbia) as a function of time using two adsorbent dosages (0.05 and 0.1 g/L). Concentration of arsenic = 150 μg/L.

These results show that a dose of 0.1 g/L of the GN-α-FeOOH aerogel could decrease the concentration of arsenic from 150 μg/L to 10 μg/L in 5 min. From this experiment, we demonstrated that, despite the chemical complexity of the natural water sample, our GN-α-FeOOH aerogel adsorbent showed practical use for the removal of arsenic from the water, which satisfied the quality standard for arsenic in drinking water recommended by WHO.

In the environmental community, the importance of scalability and sample preparation for adsorbents is often discussed. The results of this study show that the synthesis of GN-α-FeOOH aerogels starting from low-cost and available materials (graphite rocks), can be successfully demonstrated using this simple and eco-friendly process. The incorporation of iron oxide nanoparticles into the 3D graphene aerogel network significantly increases the adsorption performance of arsenic. Fast kinetics of adsorption and outstanding adsorption capacity of 81.3 mg of As(V) and 13.4 mg As(III) per gram of adsorbent is achieved, as a result of the 3D porous structure of the graphene aerogel with randomly dispersed α-FeOOH nanoparticles and its high specific surface area. The best performance for the removal of As(III) and As(V) is situated near the pH values typical for natural waters, which is excellent as this enables efficient removal without any pretreatment of the source water as supported by the results of this study. The absorbents can be prepared into different structural shapes (depending on the reaction vessel) and utilized in different forms (flat, circular, cube, etc.) for different devices, thus increasing its possibility to be applied to individual household systems where the waters are contaminated with arsenic.

■ ASSOCIATED CONTENT

Supporting Information

The information for measuring the specific surface area of the aerogel with the Methylene Blue adsorption method; figures showing the Langmuir and Freundlich plots for the sorption of As(V) and As(III); chemical composition of the tap water in the city of Zrenjanin used in the case study. This material is available free of charge via the Internet at http://pubs.acs.org.

■ AUTHOR INFORMATION

Corresponding Authors

*Tel.: + 011 3336745. E-mail: ivanhem@chem.bg.ac.rs (I. Andjelkovic).

*Tel.: +61 (8) 8313 4648. Fax: +61 (8) 8313 4373. E-mail: dusan.losic@adelaide.edu.au (D. Losic).

Author Contributions

The manuscript was written through contributions of all authors. All authors have given approval to the final version of the manuscript.

Notes

The authors declare no competing financial interest.

■ ACKNOWLEDGMENTS

This work was funded by The Australian Research Council (No. FT110100711) and The University of Adelaide, School of Chemical Engineering. The support of Valence Industries, Ltd. and Archer Exploration, Ltd. is acknowledged. I.A. acknowledges the support to the Ministry of Education and Science, Republic of Serbia (Project No. 172030). The authors also thank the technical support from Adelaide Microscopy.

■ REFERENCES

(1) Mohan, D.; Pittman, C. U., Jr. Arsenic Removal from Water/Wastewater Using Adsorbents—A Critical Review. *J. Hazard. Mater.* **2007**, *142*, 1−53.

(2) Smedley, P. L.; Kinniburgh, D. G. A Review of the Source, Behavior and Distribution of Arsenic in Natural Waters. *Appl. Geochem.* **2002**, *17*, 517−568.

(3) Shiobara, Y.; Ogra, Y.; Suzuki, K. T. Anima Species Difference in the Uptake of Dimethylarsinous Acid (DMA III) by Red Blood Cells. *Chem. Res. Toxicol.* **2001**, *14*, 1446−1452.

(4) Basu, D.; Dasgupta, J.; Mukherjee, A.; Guha Mazumder, D. N. Chronic Neuropathy due to Arsenic Intoxication from Geo-chemical Source—A Five-Year Follow Up. *J. Assoc. Neurol. Est. Ind.* **1996**, *1*, 45−47.

(5) Chen, C. J.; Hsueh, Y. M.; Lai, M. S.; Shyu, M. P.; Chen, S. Y.; Wu, M. M.; Kuo, T. L.; Tai, T. Y. Increase Prevalence of Hypertension and Long-Term Arsenic Exposure. *Hypertension* **1995**, *25* (1), 53−60.

(6) Tsuji, J. S.; Perez, V.; Garry, M. R.; Alexander, D. D. Association of Low-Level Arsenic Exposure in Drinking Water with Cardiovascular Disease: A Systematic Review and Risk Assessment. *Toxicology* **2014**, *323*, 78−94.

(7) Arain, M. B.; Kazi, T. G.; Baig, J. A.; Jamali, M. K.; Afridi, H. I.; Jalbani, N.; Sarfraz, R. A.; Shah, A. Q.; Kandhro, G. A. Respiratory Effects in People Exposed to Arsenic Via the Drinking Water and Tobacco Smoking in Southern Part of Pakistan. *Sci. Total Environ.* **2009**, *407*, 5524−5530.

(8) Tseng, C.-H. The Potential Biological Mechanisms of Arsenic-Induced Diabetes Mellitus. *Toxicol. Appl. Pharmacol.* **2004**, *197*, 67−83.

(9) Melak, D.; Ferreccio, C.; Kalman, D.; Parra, R.; Acevedo, J.; Perez, L.; Cortez, S.; Smith, A. H.; Yuan, Y.; Liaw, J.; Steinmaus, C. Arsenic Methylation and Lung and Bladder Cancer in a Case-Control Study in Northern Chile. *Toxicol. Appl. Pharmacol.* **2014**, *274*, 225−231.

DOI: 10.1021/acsami.5b01624
ACS Appl. Mater. Interfaces 2015, 7, 9758−9766

(10) Wang, W.; Cheng, S.; Zhang, D. Association of Inorganic Arsenic Exposure with Liver Cancer Mortality: A Meta-Analysis. *Environ. Res.* **2014**, *135*, 120−125.
(11) Hunt, K. M.; Srivastava, R. K.; Elmets, C. A.; Athar, M. The Mechanistic Basis of Arsenicosis: Pathogenesis of Skin Cancer. *Cancer Lett.* **2014**, *354*, 211−219.
(12) Hering, J. G.; Kneebone, P. E. *Environmental Chemistry of Arsenic*; Marcel Dekker: New York, 2002.
(13) Xu, Y. H.; Nakajima, T.; Ohki, A. Adsorption and Removal of Arsenic(V) from Drinking Water by Aluminum-Loaded Shirasu-Zeolite. *J. Hazard. Mater.* **2002**, *92*, 275−287.
(14) Wang, S.; Peng, Y. Natural Zeolites as Effective Adsorbents in Water and Wastewater Treatment. *Chem. Eng. J.* **2010**, *156*, 11−24.
(15) Kartinen, E. O., Jr.; Martin, C. J. An Overview of Arsenic Removal Processes. *Desalination* **1995**, *130* (1−2), 79−88.
(16) World Health Organization (WHO). *Guidelines for Drinking-Water Quality*, 2nd Edition. Presented at the WHO Conference, Geneva, Switzerland, 1998.
(17) Singh, T. S.; Pant, K. K. Equilibrium, Kinetics and Thermodynamic Studies for Adsorption of As(III) on Activated Alumina. *Sep. Purif. Technol.* **2004**, *36*, 139−147.
(18) Pena, M. E.; Korfiatis, G. P.; Patel, M.; Lippincott, L.; Meng, X. Adsorption of As(V) and As(III) by Nanocrystalline Titanium Dioxide. *Water Res.* **2005**, *39*, 2327−2337.
(19) Zhang, J.; Stanforth, R. Slow Adsorption Reaction Between Arsenic Species and Goethite (α-FeOOH): Diffusion or Heterogeneous Surface Reaction Control. *Langmuir* **2005**, *21*, 2895−2901.
(20) Faria, M. C. S.; Rosemberg, R. S.; Bomfeti, C. A.; Monteiro, D. S.; Barbosa, F.; Oliveira, L. C. A.; Rodriguez, M.; Pereira, C. M.; Rodrigues, J. L. Arsenic Removal from Contaminated Water by Ultrafine δ-FeOOH Adsorbents. *Chem. Eng. J.* **2014**, *237*, 47−54.
(21) Lafferty, B. J.; Loeppert, R. H. Methyl Arsenic Adsorption and Desorption Behavior on Iron Oxides. *Environ. Sci. Technol.* **2005**, *39*, 2120−2127.
(22) Lorenzen, L.; van Deventer, J. S. J.; Landi, W. M. Factors Affecting the Mechanism of the Adsorption of Arsenic Species on Activated Carbon. *Miner. Eng.* **1995**, *8*, 557−569.
(23) Rajaković, L. V. The Sorption of Arsenic onto Activated Carbon Impregnated with Metallic Silver and Copper. *Sep. Purif. Technol.* **1992**, *27*, 1423−1433.
(24) Elizalde-González, M. P.; Mattusch, J.; Einicke, W. D.; Wennrich, R. Sorption on Natural Solids for Arsenic Removal. *Chem. Eng. J.* **2001**, *81*, 187−195.
(25) Wang, Y.; Tsang, D. C. W. Effects of Solution Chemistry on Arsenic(V) Removal by Low-Cost Adsorbents. *J. Environ. Sci.* **2013**, *25*, 2291−2298.
(26) Sasaki, T.; Iizuka, A.; Watanabe, M.; Hongo, T.; Yamasaki, A. Preparation and Performance of Arsenate(V) Adsorbents Derived from Concrete Wastes. *Waste Manage.* **2015**, *34*, 1829−1835.
(27) Hu, X.; Ding, Z.; Zimmerman, A. R.; Wang, S.; Gao, B. Batch and Column Sorption of Arsenic onto Iron-Impregnated Biochar Synthesized Through Hydrolysis. *Water Res.* **2014**, *68*, 206−216.
(28) Zhu, Y.; Murali, S.; Cai, W.; Li, X.; Suk, J. W.; Potts, J. R.; Ruoff, R. S. Graphene and Graphene Oxide: Synthesis, Properties, and Applications. *Adv. Mater.* **2010**, *22* (35), 3906−3924.
(29) Geim, A. K.; Novoselov, K. S. The Rise of Graphene. *Nat. Mater.* **2007**, *6*, 183−191.
(30) Novoselov, K. S.; Jiang, D.; Schedin, F.; Booth, T. J.; Khotkevich, V. V.; Morozov, S. V.; Geim, A. K. Two Dimensional Atomic Crystals. *Proc. Natl. Acad. Sci. U.S.A* **2005**, *102*, 10451−10453.
(31) Chandra, V.; Park, J.; Chun, Y.; Lee, J. W.; Hwang, I. C.; Kim, K. S. Water-Dispersible Magnetite-Reduced Graphene Oxide Composites for Arsenic Removal. *ACS Nano* **2010**, *4*, 3979−3986.
(32) Zhang, K.; Dwivedi, V.; Chi, C.; Wu, J. Graphene Oxide/Ferric Hydroxide Composites for Efficient Arsenate Removal from Drinking Water. *J. Hazard. Mater.* **2010**, *182*, 162−180.
(33) Saleh, T. A.; Agarwal, S.; Gupta, V. K. Synthesis of MWCNT/MnO_2 and Their Application for Simultaneous Oxidation of Arsenite and Sorption of Arsenate. *Appl. Catal., B* **2011**, *106*, 46−53.
(34) Nandi, D.; Gupta, K.; Ghosh, A. K.; De, A.; Banerjee, S.; Ghosh, U. C. Manganese-Incorporated Iron(III) Oxide-Graphene Magnetic Nanocomposite: Synthesis, Characterization, and Application for the Arsenic(III)-Sorption from Aqueous Solution. *J. Nanopart. Res.* **2012**, *14*, 1272−1285.
(35) Yao, S.; Jia, Y.; Shi, Z.; Zhao, S. Photocatalytic Oxidation of Arsenite by a Composite of Titanium Dioxide and Activated Carbon Fiber. *Photochem. Photobiol.* **2010**, *86*, 1215−1221.
(36) Cong, H.-P.; Ren, X.-C.; Wang, P.; Yu, S.-H. Macroscopic Multifunctional Graphene-Based Hydrogels and Aerogels by a Metal Ion Induced Self-Assembly Process. *ACS Nano* **2012**, *6*, 2693−2703.
(37) Kabiri, S.; Tran, D. N. H.; Altalhi, T.; Losic, D. Outstanding Adsorption Performance of Graphene-Carbon Nanotube Aerogels for Continuous Oil Removal. *Carbon* **2014**, *80*, 523−533.
(38) Rao, C. N. R.; Sood, A. K.; Subrahmanyam, K. S.; Govindaraj, A. Graphene: The New Two-Dimensional Nanomaterial. *Angew. Chem., Int. Ed.* **2009**, *48*, 7752−7777.
(39) Marcano, D. C.; Kosynkin, D. V.; Berlin, J. M.; Sinitskii, A.; Sun, Z.; Slesarev, A.; Alemany, L. B.; Lu, W.; Tour, J. M. Improved Synthesis of Graphene Oxide. *ACS Nano* **2010**, *4*, 4806−4814.
(40) Yukselen, Y.; Kaya, A. Suitability of the Methylene Blue Test for Surface Area, Cation Exchange Capacity and Swell Potential Determination of Clayey Soils. *Eng. Geol.* **2008**, *102*, 38−45.
(41) Montes-Navajas, P.; Asenjo, N. G.; Santamaría, R.; Menéndez, R.; Corma, A.; García, H. Surface Area Measurement of Graphene Oxide in Aqueous Solutions. *Langmuir* **2013**, *29*, 13443−13448.
(42) Kuila, T.; Bose, S.; Mishra, A. K.; Khanra, P.; Kim, N. H.; Lee, J. H. Chemical Functionalization of Graphene and its Application. *Prog. Mater. Sci.* **2012**, *57*, 1061−1105.
(43) Kudin, K. N.; Ozbas, B.; Prud'homme, R. K.; Aksay, I. A.; Car, R. Raman Spectra of Graphite Oxide and Functionalized Graphene Sheets. *Nano Lett.* **2008**, *8*, 36−41.
(44) Zhang, C.; Zhu, J.; Rui, X.; Chen, J.; Sim, D.; Shi, W.; Hng, H. H.; Lim, T. M.; Yan, Q. Synthesis of Hexagonal-Symmetry α-Iron Oxyhydroxide Crystals Using Reduced Graphene Oxide as a Surfactant and Their Li Storage Properties. *CrystEngComm* **2012**, *14*, 147−153.
(45) Ho, Y. S. Citation Review of Lagergren Kinetic Rate Equation on Adsorption Reactions. *Scientometrics* **2004**, *59*, 171−177.
(46) Ho, Y. S.; Ng, J. C. Y.; McKay, G. Kinetics of Pollutant Sorption by Biosorbents: Review. *Sep. Purif. Methods* **2000**, *29*, 189−232.
(47) McKay, G.; Ho, Y. S.; Ng, J. C. Y. Biosorption of Copper from Waste Waters: A Review. *Sep. Purif. Rev.* **1999**, *28*, 87−125.
(48) Zhang, G.; Qu, J.; Liu, H.; Liu, R.; Wu, R. Preparation and evaluation of a novel Fe-Mn binary oxide adsorbent for effective arsenite removal. *Water Res.* **2007**, *41*, 1921−1928.
(49) Wang, S.; Mulligan, C. N. Occurrence of Arsenic Contamination in Canada: Sources, Behavior and Distribution. *Sci. Total Environ.* **2006**, *366*, 701−721.
(50) Escudero, C.; Fiol, N.; Villaescusa, I.; Bollinger, J.-C. Arsenic Removal by a Waste Metal (Hydr)oxide Entrapped into Calcium Alginate Beads. *J. Hazard. Mater.* **2009**, *164*, 533−541.
(51) Jeon, C.-S.; Baek, K.; Park, J.-K.; Oh, Y.-K.; Lee, S.-D. Adsorption Characteristics of As(V) on Iron-Coated Zeolite. *J. Hazard. Mater.* **2009**, *163*, 804−808.
(52) Arcibar-Orozco, J. A.; Delgado-Balbuena, J.; Rios-Hurtado, J. C.; Rangel-Mendez, J. R. Influence of Iron Content, Surface Area, Charge Distribution in the Arsenic Removal by Activated Carbons. *Chem. Eng. J.* **2014**, *249*, 201−209.
(53) Freundlich, H. M. F. Über Die Adsorption in Lösungen. *Z. Phys. Chem.* **1906**, *57A*, 385−470.
(54) Langmuir, I. The Constitution and Fundamental Properties of Solids and Liquids. Part I. Solids. *J. Am. Chem. Soc.* **1916**, *38*, 2221−2295.
(55) Luo, X.; Wang, C.; Luo, S.; Dong, R.; Tu, X.; Zeng, G. Adsorption of As(III) and As(V) from Water Using Magnetite Fe_3O_4−Reduced Graphite Oxide−MnO_2 Nanocomposites. *Chem. Eng. J.* **2012**, *187*, 45−52.

DOI: 10.1021/acsami.5b01624
ACS Appl. Mater. Interfaces 2015, 7, 9758−9766

(56) Zhang, S.; Li, X.-Y.; Chen, J. P. Preparation and Evaluation of a Magnetite-Doped Activated Carbon Fiber for Enhanced Arsenic Removal. *Carbon* **2010**, *48*, 60−67.
(57) Wu, X.-L.; Wang, L.; Chen, C.-L.; Xu, A.-W.; Wang, X.-K. Water-Dispersible Magnetite−Graphene−LDH Composites for Efficient Arsenate Removal. *J. Mater. Chem.* **2011**, *21*, 17353−17359.

DOI: 10.1021/acsami.5b01624
ACS Appl. Mater. Interfaces 2015, 7, 9758−9766